

Original Research

N_2O Abatement over Ruthenium Supported on Highly Dispersed Hydrotalcite-Like Composite Metal Oxides

Yuanyang Zhang, Yaqiong Guo, Na Li, Yaoyu Feng*

School of Resources and Environmental Engineering, East China University of Science and Technology, Shanghai, China

Received: 7 June 2018

Accepted: 8 September 2018

Abstract

Highly dispersive hydrotalcite-like composite metal oxides were prepared by coprecipitation method. CO_2 -TPD characterization showed that the adsorption capacity over the samples at low ($<300^\circ C$) and middle ($300\sim 550^\circ C$) temperatures was improved by using La or Cu to modify the sample of $MgAlO$, while slightly reduced at high temperature ($>550^\circ C$). The experimental results showed that the composite metal oxide, Me_xO_y (Me=La, Mg, Al), had relatively good performance on N_2O decomposition. A series of Ru/Me_xO_y catalysts were prepared by programmed impregnation method. CO_2 -TPD analysis indicated that the samples of Ru/Me_xO_y not only increased the total CO_2 adsorption capacity, but also obviously enhanced CO_2 adsorption capacity at $300\sim 550^\circ C$ compared with Me_xO_y . TEM characterization showed that the Ru component was uniformly loaded on the support surface under nanoscale. N_2O catalytic decomposition showed that the suitable Ru loading on support was 2.0(wt.-%), i.e., $Ru(2.0)/Me_xO_y$. Under conditions of (v/v) 10% N_2O +82% N_2 +5.0% O_2 +3.0% H_2O , 30000 h^{-1} of space velocity, $510^\circ C$, the stability test showed that N_2O conversion remained *ca.* 95.0%, indicating that $Ru(2.0)/Me_xO_y$ had good stability and activity at relatively low temperature.

Keywords: N_2O abatement; composite metal oxides; hydrotalcite-like structure; coprecipitation; programmed impregnation

Introduction

It has been reported that the global warming potential of N_2O is approximately 300 times higher than that of CO_2 , and N_2O also shows a long lifetime in the atmosphere (almost 150 years). In addition, its potential for depleting the stratospheric ozone layer is comparable to that of hydrochlorofluorocarbons

(HCFCs), known as the most important ozone-depleting agents [1,2]. However, the average rate of increase of the N_2O levels in the atmosphere is still approximately 0.2~0.3% annually, which is mainly caused by human activity, such as adipic and nitric acid plants as well as fuel combustion processes, especially after the 1980s [3-5]. Therefore, more research has not only paid much attention to the study of the effects of N_2O on the environment and human body, but also has focused on the effective control of N_2O emissions from stationary and mobile processes [6-9]. Several technologies have been potentially developed for N_2O abatement,

*e-mail: proffengyy@126.com

including thermal decomposition (TDeN₂O) [10], nonselective catalytic reduction (NCR) [11], selective catalytic reduction (SCR) [12, 13], and direct catalytic decomposition (DeN₂O) [14]. In addition, techniques using N₂O as an oxidant to catalyze benzene to phenol (OBPh) are also very interesting [15]. However, it is believed that the DeN₂O approach is the most promising method due to its efficiency and low energy requirements.

Various catalytic systems such as transition and noble catalysts, perovskites, spinels and zeolites have been widely reported [16–21]. Yentekakis et al. [22] used iridium as a catalytic component and it was supported on a variety of surfaces, e.g., γ -Al₂O₃ and composites of gadolinia-ceria, alumina-ceria-zirconia, indicating that the composites exhibited high resistance of the iridium nanoparticles to sintering in an oxidative environment, and that the catalytic behavior was consistent with the independently measured sintering characteristics, while Lin et al. [23] reported that the Ir/Al₂O₃ sample exhibited excellent performance in initiating the decomposition of N₂O at a low temperature of 200°C. Abu-Zied et al. [24] recently indicated that the samples of rare earth (Nd, Pr, Tb and Y) doped NiO prepared by the calcination of their corresponding oxalate mixtures, which were synthesized via the microwave-assisted precipitation method, had led to an obvious decrease of the NiO crystallites size, and it was the origin of a substantial activity increase upon doping NiO with the various rare earth oxides. Basahel et al. [25] showed that the addition of a small amount of ZrO₂ to Zn/Co-mixed spinel could improve its activity on N₂O decomposition, which could be ascribed to the fact that Zr⁴⁺-doped samples not only stabilized the ZnCo₂O₄ phase and suppressed the formation of the ZnO phase at the temperatures from 550°C to 750°C, but is also related to the increased Co²⁺/Co³⁺ redox couple content. Its activity could be further improved by a suitable addition of CeO₂ to Zn-Co-O mixed oxide, which could be the reason for the eventual promotion of the reduction of Co³⁺ to Co²⁺ [26]. Eom et al. [27] indicated that various forms of cobalt oxide (Co₃O₄ and Co₂O₃) as well as modified with alkali metal (10% Na) and alkaline earth metal (10% Ba) were inactive for N₂O decomposition, while these samples became very active for N₂O decomposition when reduced under reduction media (H₂ gas), probably due to the oxidation state change of cobalt oxides during the reduction process. However, Kim et al. [28] found that an alkali metal modified sample (K/Co₃O₄) showed notable activity on N₂O decomposition, and its performance could be further improved with the suitable addition of CeO₂ (K/Co-CeO₂). Zhang et al. [29] used potassium or sodium oxide to modify the Zn/Mg-Co catalyst and found that the catalyst activity for N₂O decomposition was improved. Characterization indicated that the addition of potassium or sodium oxide decreased the binding energy and resulted in an increase in the density of the electron cloud around Co and an improvement of catalytic activity. Grzybek et

al. [30] found that the (Co, Zn)Co₂O₄/CeO₂/cordierite catalyst prepared by the impregnation method gave good performance for N₂O decomposition with the help of dispersion of the active spinel phase over the cordierite. Zabilskiy et al. [31] recently reported the performance of a series of CuO/CeO₂ catalysts prepared by impregnation method for N₂O decomposition. It was found that the sample containing 10(wt.%) of Cu showed the best activity on N₂O degradation, which could be attributed to the highest number of small CuO clusters on the catalyst surface and the synergistic interaction between copper and ceria [32]. The catalyst activity, however, was found to be degraded in the presence of small amounts of oxygen and water vapor in the feed stream [33]. Zheng et al. [34] used zinc oxide to replace CeO₂ and supported ZnAl₂O₄, indicating that Cu-Zn/ZnAl₂O₄ showed higher catalytic performance along with good stability during N₂O decomposition by using the mixture (v/v) 8.1% N₂O+10.2% O₂+balanced N₂ at atmosphere. Liu et al. [35] reported that the mixed metal oxides with molar ratio of Ni/Ce by 8.0/1.0, denoted Ni₈Ce₁, prepared by hydrothermal method showed good activity and stability on N₂O decomposition at 450°C by using the model mixtures (v/v) 0.2% N₂O+2.0% O₂+balanced He.

The studies of the various N₂O decomposition catalysts described above have mostly focused on the use of transition metal oxides as the main catalytic components, which were usually modified by using alkali and alkaline earth metals or rare-earth metals. Catalysts related to Co-Me (Me = Zn, Cu, Ce) or Cu-Ce have been mostly investigated. However, due to the cobalt's negative effect on the environment during the process of industrial catalyst manufacturing as well as the degradation of the Cu-Ce catalyst activity in the presence of oxygen and water vapor in the feed stream, it is still interesting and challenging to explore novel catalysts potentially applying for effective catalytic N₂O decomposition. This paper reports that the high dispersive hydrotalcite-like composite metal oxides, Me_xO_y (Me = La, Mg, Al), modified with Ru oxides by using programmed impregnation method, show good stability and activity at relatively low temperature, which provides the basis for further pilot-scale study for potential application in industries.

Material and Methods

Sample Preparation

The high dispersive hydrotalcite-like composite metal oxides were prepared by coprecipitation method. A prepared solution containing Na₂CO₃ and NaOH was added dropwise to a solution containing known amounts of Al(NO₃)₃, Mg(NO₃)₂, Cu(NO₃)₂, Zn(NO₃)₂, Zr(NO₃)₄, Mn(NO₃)₂ or La(NO₃)₃ (C.P. grade, China) under stirring at ca. 70°C until the pH of the solution reached ca. 9.0. The resulting precipitate was aged at 70–90°C

overnight, and then filtered, washed with distilled water until the pH of the filtrate was ca. 7.0, and dried at 105°C overnight, followed by calcination in a muffle furnace for 4~6h at 530°C in static air. Afterward, a series of ruthenium-supported catalysts were prepared by using the suitable hydroxalcite-like composite metal oxide as the support and programmed impregnation method, in which the RuCl₃·xH₂O (C.P. grade, China) was used as the precursor of Ru active component.

Characterization

The specific surface area and pore structure of the prepared samples were analyzed at -196°C over a range of relative pressures through nitrogen adsorption-desorption isotherms performed on an automated ASAP 2020 instrument (Micromeritics Corporation, USA). The compositions of catalytic components for typical samples were analyzed by inductively coupled plasma-atomic emission spectroscopy (ICP-AES) (Varian 710-ES, USA). Fourier transform infrared spectra (FT-IR) were performed on Nicolet NEXUS 470 (USA) spectrometer equipped with a DTGS detector. Structural characterization via X-ray diffractometry (XRD) was performed on a computerized Rigaku D/max-RB diffractometer (Japan, CuK α radiation, $\lambda = 0.154$ nm, 50 kV, 40 mA) over a 2θ range of 5~80° with a step of 4°/min. The surface morphology (SEM) of the samples was characterized by using an FEI Quanta 400 FEG ESEM (15kV) electron microscope (USA), and an energy dispersive spectrometer (EDS) was used to confirm the nature of the components on the surface. The typical supported Ru samples were characterized by using the transmission electron microscopy (TEM) (Japanese, JEM-2010HR, operated at 200kV). The physicochemical properties of the sample surface were determined by using a TP-5080 multi-functional automatic adsorption instrument (China) with CO₂ temperature-programmed desorption (CO₂-TPD). A particle size analyzer of S3500-BWD (Microtrac, USA) was also used to identify the particle size distribution of composite metal oxides prepared by coprecipitation method.

Activity Evaluation

The experiments on catalytic N₂O abatement were carried out in a laboratory fixed-bed micro reactor

using approximately 1.0 g of catalyst for each test. Before testing, the sample loaded in the reactor was pretreated with a mixture of N₂ and O₂ at 500°C for approximately 1.0h to yield a clean surface. Then the temperature of the reactor was controlled at the testing temperature. Afterward, the reactant mixture containing N₂O with an hourly space velocity in the range of 10000~40000 h⁻¹ was used to evaluate the sample performance on N₂O decomposition. The reaction system was maintained for 1 h at each reaction temperature so that the system could reach a steady state to obtain reliable N₂O conversion data. The tested temperature range was varied from 150°C to 700°C for each sample. The composition of the outlet mixture was analyzed by an online gas chromatograph (GC-2010 PLUS, Shimadzu, Japan) equipped with HP-PLOT/Q capillary columns (30 m × 0.32 mm × 20 μ m) and an ECD detector. The catalyst performance was expressed as N₂O conversion under the applied experimental conditions, which was calculated based on the N₂O concentrations at the inlet and outlet, respectively.

Results and Discussion

Hydroxalcite-Like Composite Metal Oxides

BET and ICP Characterization

The composition, specific surface area and average pore size characterized by BET and ICP over the composite metal oxides prepared by coprecipitation method are listed in Table 1, which indicates that the molar composition of the active components of the prepared samples were close to the designed value. The specific surface area and pore size for all samples was ca. 50 m²/g and 8~12 nm, respectively. In addition, the distribution of particle size measured by laser particle size analyzer for the precursors prepared by coprecipitation method was ca. 0.8~2 μ m under applied preparation conditions.

FT-IR Characterization

FT-IR characterization over LaMgAlO samples before and after calcination prepared by the precipitation method are shown in Fig. 1. This indicated

Table 1. ICP and BET results over samples prepared by coprecipitation method.

Samples	Calcined temperature (°C)	ICP	BET	
		Molar composition	Surface area (m ² /g)	Pore size (nm)
MgAlO	530	Mg/Al \approx 3.0	48	8.6
CuMgAlO	530	Cu/(Cu+Mg+Al) \approx 0.1	39	11
ZrMnZnO	530	Zr/(Zr+Mn+Zn) \approx 0.1	45	12
LaMgAlO	530	La/(La+Mg+Al) \approx 0.1	51	9.8

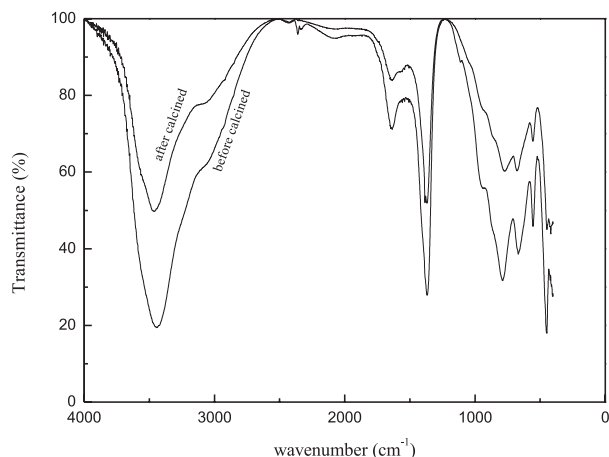


Fig. 1. FT-IR characterization of LaMgAlO precursor before and after calcinations at high temperature.

that the characteristic peaks for the sample before calcination mainly appeared in 3400 cm^{-1} , 1630 cm^{-1} , 1350 cm^{-1} , 750 cm^{-1} , 630 cm^{-1} , 530 cm^{-1} and 430 cm^{-1} . The wide characteristic peak ca. 3400 cm^{-1} belonged to the stretch and flexural vibration of the water molecule at interlayer, and the characteristic peak ca. 1600 cm^{-1} belonged to the bending vibration of OH^- for the crystallized water, and 1350 cm^{-1} characteristic peak was attributable to the C-O asymmetric stretch vibration of CO_3^{2-} , indicating that it was shifted to the low wave number compared with the free OH^- (ca. 3600 cm^{-1}) and CO_3^{2-} (1430 cm^{-1}), which was probably a result of the interaction between the crystallized water and CO_3^{2-} at interlayer of the hydrotalcite-like structure. Furthermore, the characteristic peaks among the region of $700\sim 400\text{ cm}^{-1}$ belonged to M-O vibration of the composite metal oxides. Similar characteristic peaks appeared in the sample calcinated at 530°C , which indicated that the LaMgAlO sample prepared by precipitation method after calcination also remained the hydrotalcite-like structure. However, it showed that the characteristic peaks over calcinated LaMgAlO sample appeared in ca. 1600 cm^{-1} for OH^- of the crystallized water and ca. 1350 cm^{-1} for C-O of CO_3^{2-} were obviously weakened compared with the sample before calcination, respectively, which indicated that although the samples before and after calcination remained somewhat similar while the microstructure and composition of the samples had been changed, the physical and chemical properties of the samples would also be different. In addition, the other samples prepared by the coprecipitation method also showed similar results to the LaMgAlO sample.

XRD Characterization

XRD characterization over the prepared samples is shown in Fig. 2, which indicates that the spinel diffraction peak of MgAl_2O_4 appeared in the MgAlO

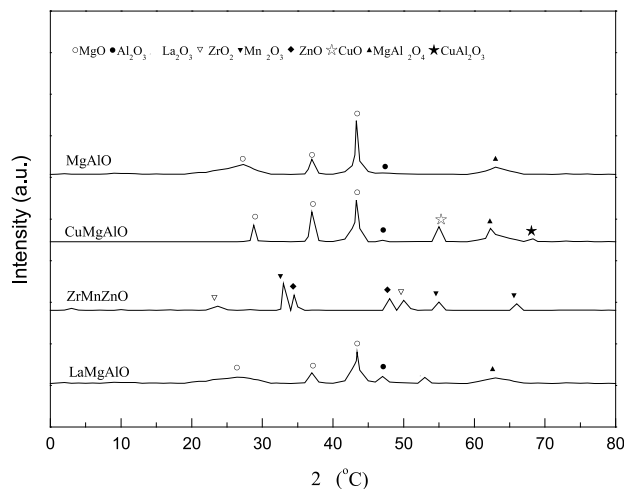


Fig. 2. XRD characterization results over samples prepared by co-precipitation method.

sample besides the main diffraction peak of MgO and Al_2O_3 . The diffraction peak of CuAl_2O_4 spinel structure appeared in the CuMgAlO sample calcinated at 530°C . With respect to ZrMnZnO and LaMgAlO samples, the obtained results indicated that it only showed characteristic peaks of single metal oxides, i.e., ZrO_2 , Mn_2O_3 , ZnO, or La_2O_3 , respectively, without composite spinel structure formed when calcinated at 530°C under used preparation conditions.

CO_2 -TPD Characterization

CO_2 -TPD characterization showed that the adsorbed CO_2 on the surface of the composite metal oxides could be divided into three states: temperature below 300°C ($<300^\circ\text{C}$), middle temperature ($300\sim 550^\circ\text{C}$), and temperature above 550°C ($>550^\circ\text{C}$) (Fig. 3). This indicates that the surface over MgAlO sample

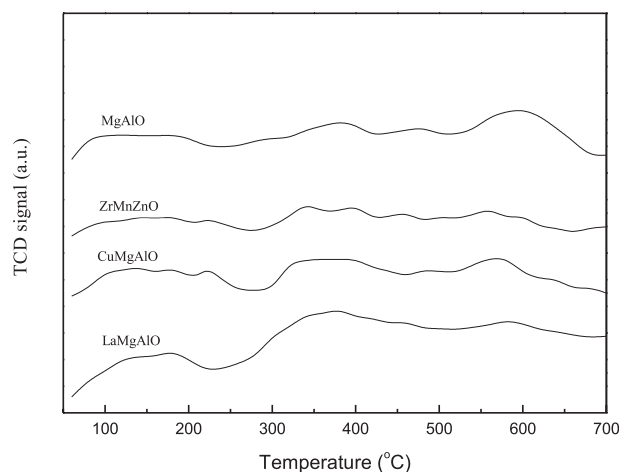


Fig. 3. CO_2 -TPD characterization over samples prepared by coprecipitation method.

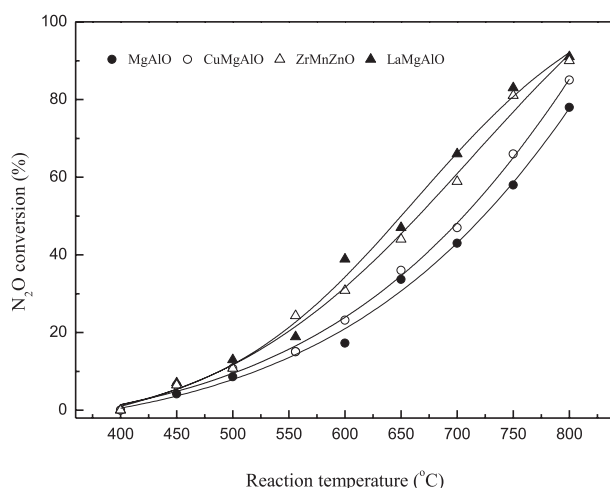


Fig. 4. Comparison of N₂O conversion over samples prepared by coprecipitation method.

appeared in a relatively strong desorbed CO₂ characteristic peak at high temperature above 550°C, while the characteristics of surface alkaline would be inevitably changed by using metal oxides of La₂O₃ or Cu₂O/CuO to modify the sample of MgAlO under applied preparation conditions, indicating that the modified samples (CuMgAlO, LaMgAlO) had enhanced its adsorbed ability on CO₂ at low temperature while being weakened at high temperature, respectively. However, the sample of ZrMnZnO showed a relatively weak wide characteristic peak in the temperature range of 300~600°C, probably indicating the interaction among various active components on the sample.

N₂O Decomposition

Fig. 4 showed the N₂O conversion over different hydrotalcite-like composite metal oxides under the following experimental conditions, gas mixture (v/v) 37% N₂O+40% N₂+20% O₂+3.0% H₂O, 10000 h⁻¹ of space velocity. This indicated that the activity was not very different when the reaction temperature was below 500°C, while its activity had been improved when samples modified with different active components compared with the MgAlO sample when the reaction

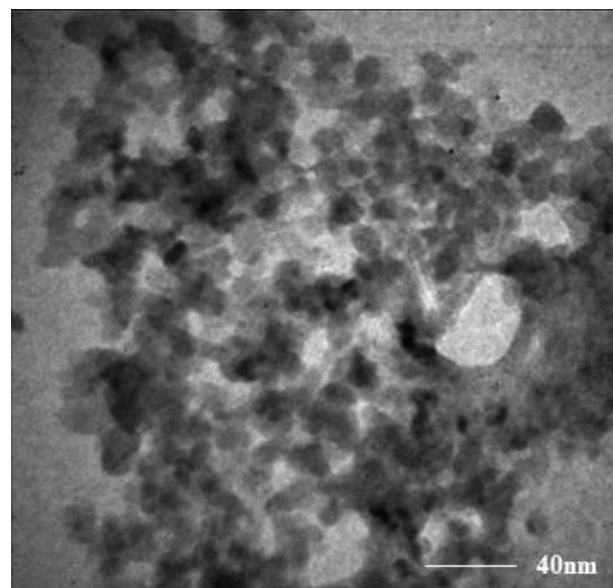


Fig. 5. TEM characterization of Me_xO_y sample supported with ruthenium calcined at 380°C.

temperature was above 500°C. The activity order over samples was followed by LaMgAlO>ZrMnZnO>CuMgAlO>MgAlO under applied experimental conditions, which was basically consistent with the variation of surface alkaline characteristics (Fig. 3). In addition, the stability test over the LaMgAlO sample indicated that it had relatively good activity and stability under applied experimental conditions, 10000 h⁻¹ of space velocity, reaction temperature of 600°C, the same reactant gas mixture as above, and lasted for 120 h, which provided the theoretical and experimental basis for further research on improving sample activity.

Preparing Ru/Me_xO_y Catalysts

The above results showed that the hydrotalcite-like composite metal oxide, LaMgAlO (Me_xO_y), had relatively good performance on N₂O decomposition, while its activity on N₂O decomposition was not good enough under used experimental conditions. Therefore, a series of Ru/Me_xO_y catalysts were prepared by

Table 2. ICP and BET results over ruthenium-supported samples.

Samples	Calcined temperature (°C)	BET		
		ICP Ru content (wt%)	Surface area (m ² /g)	Pore size (nm)
Ru (0.5)/ Me _x O _y	380	0.5	48	9.5
Ru (1.0)/ Me _x O _y	380	1.0	46	9.4
Ru (1.5)/ Me _x O _y	380	1.5	45	9.6
Ru (2.0)/ Me _x O _y	380	2.0	43	8.9
Ru (3.0)/ Me _x O _y	380	3.0	43	9.1

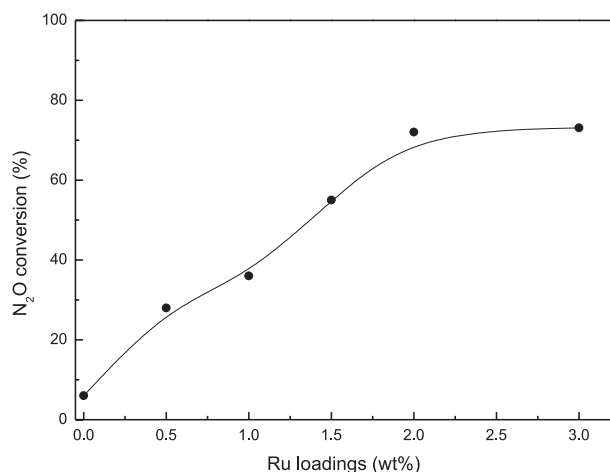


Fig. 6. Effect of Ru loadings on N₂O decomposition over supported Ru/Me_xO_y catalysts.

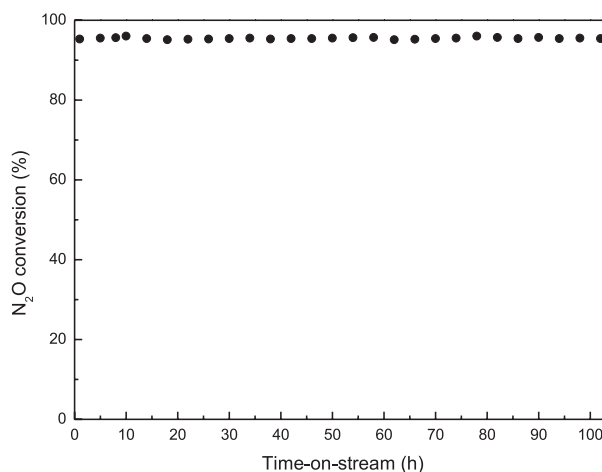


Fig. 7. Variation of N₂O conversion over Ru (2.0)/Me_xO_y catalyst as a function of time-on-stream.

programmed impregnation method in order to further improve its activity on N₂O decomposition.

ICP and BET Analysis

ICP and BET results over Ru/Me_xO_y samples were listed in Table 2, which indicated that the loading of Ru on the Me_xO_y support was in the range of 0.5~3.0 (wt)%. BET analysis indicated that the specific surface area of Ru/Me_xO_y samples was slightly decreased with the increase of the loading Ru on the support, indicating the influence of the supported catalyst on the pore structure of the support, Me_xO_y, was not obvious by using the programmed impregnation method.

TEM Characterization

TEM characterization over 2.0(wt)% Ru/Me_xO_y sample, i.e., Ru(2.0)/Me_xO_y, calcinated at 380°C was shown in Fig. 5, which showed that the Ru component was uniformly loaded on the support surface under nanoscale, indicating that the preparation method was suitable and could fully make use of the ruthenium active component on N₂O abatement.

Ru/Me_xO_y Performance on N₂O Decomposition

Fig. 6 showed the variation of N₂O conversion over Ru/Me_xO_y samples with Ru loadings on Me_xO_y support under the following conditions: gas mixture (v/v) 37% N₂O+40% N₂+20% O₂+3.0% H₂O, 30000 h⁻¹ of space velocity, reaction temperature 450°C. This indicated that the activity of Ru/Me_xO_y samples was obviously increased with the loading of Ru when the content of Ru on support was below 2.0(wt)%, while the activity was not continuously increased when Ru loading was above 2.0(wt)% under applied experimental conditions, indicating that the suitable Ru loading on the hydrotalcite-like composite metal oxide, Me_xO_y, was ca. 2.0(wt)%, which not only made the prepared sample, Ru(2.0)/Me_xO_y, have good activity on N₂O decomposition but also saved the cost of catalyst production for potential industrial applications.

Table 3 lists the results of CO₂-TPD characterization over support, Me_xO_y, and these ruthenium-supported catalysts, Ru/Me_xO_y, respectively. Results indicated that the supported catalysts of Ru/Me_xO_y reduced the CO₂ adsorption capacity at low temperature (<300°C), while obviously increasing at the middle temperature (300~550°C) and high temperature (>550°C) compared

Table 3. Basicity and its distribution over Ru/Me_xO_y samples compared with Me_xO_y.

Samples	Amount of total basic sites (μmol g ⁻¹)	Distribution of different basic sites (%)		
		<300°C	300~550°C	>550°C
Me _x O _y (support)	129	23.2	47.2	29.4
Ru (0.5)/ Me _x O _y	147	9.5	55.7	34.6
Ru (1.0)/ Me _x O _y	166	6.6	57.2	36.1
Ru (1.5)/ Me _x O _y	186	4.3	58.1	37.6
Ru (2.0)/ Me _x O _y	224	2.2	59.8	37.9
Ru (3.0)/ Me _x O _y	229	1.7	58.9	39.3

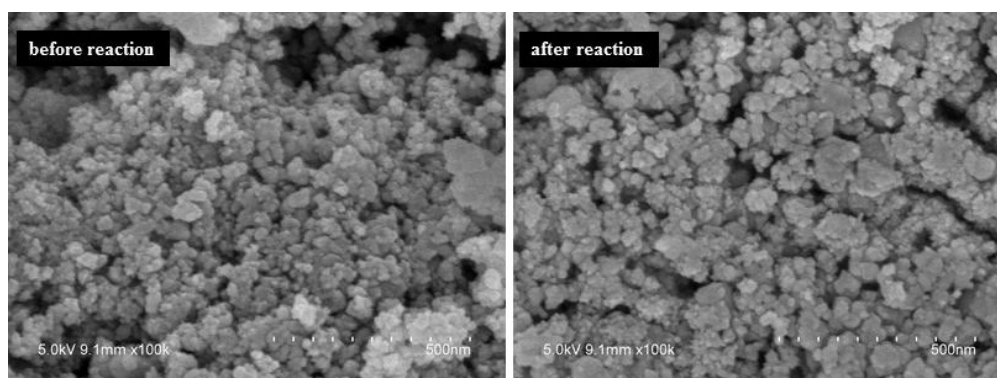


Fig. 8. Comparison of surface morphology over Ru(2.0)/Me_xO_y samples before and after reaction.

with the Me_xO_y sample. Furthermore, the total adsorbed CO₂ capacity on the surface of Ru/Me_xO_y samples was obviously increased compared with the Me_xO_y sample, indicating that it was probably the origin of Ru/Me_xO_y catalysts that had good activity compared with the Me_xO_y sample under similar applied experimental conditions.

Stability Test over Ru(2.0)/Me_xO_y Catalyst

Fig. 7 showed the stability result over Ru(2.0)/Me_xO_y catalyst under the following applied conditions, gas mixture (v/v) 10% N₂O+82% N₂+5.0% O₂+3.0% H₂O, 30000 h⁻¹ of space velocity, and 510°C. It indicated that the Ru(2.0)/Me_xO_y catalyst had good stability when the reactant mixture contained small amounts of oxygen and water vapor. The N₂O conversion was stable and more than 95% during the period of stability test lasted for over 100h, which also implied that the Ru(2.0)/Me_xO_y catalyst had good activity at low temperature. The preliminary results provided the basis for further pilot scale study for potential industrial applications.

SEM Characterization over Samples before and after Reaction

SEM characterization over Ru(2.0)/Me_xO_y catalysts before and after reaction is shown in Fig. 8, which indicates that the surface of the used Ru(2.0)/Me_xO_y sample was slightly rough compared with the fresh Ru(2.0)/Me_xO_y sample, while it did not affect its activity on N₂O decomposition under applied experimental conditions (Fig. 7), indicating that the prepared Ru(2.0)/Me_xO_y catalyst had good stable structure when the reactant mixture contained small amounts of oxygen and water vapor.

Conclusions

CO₂-TPD characterization over hydrotalcite-like composite metal oxides prepared by the coprecipitation method showed that the adsorption capacity over the

samples at low temperature (<300°C) and middle temperature (300~550°C) were improved by using La or Cu to modify the sample of MgAlO, while being slightly reduced at high temperature (>550°C). Results indicated that the LaMgAlO (Me_xO_y) sample had relatively good performance on N₂O decomposition. A series of Ru/Me_xO_y catalysts were prepared by programmed impregnation method. CO₂-TPD characterization showed that the samples of Ru/Me_xO_y not only increased total CO₂ adsorption capacity, but also obviously enhanced CO₂ adsorption capacity at 300~550°C compared with Me_xO_y. TEM characterization indicated that the Ru component was uniformly loaded on the support surface under nanoscale, indicating that the preparation method was suitable and could make full use of ruthenium active component on N₂O abatement. Catalytic N₂O decomposition showed that the suitable Ru loading on the support was 2.0(wt.%) , i.e., Ru(2.0)/Me_xO_y. The stability test showed that N₂O conversion remained ca. 95.0%, indicating that Ru(2.0)/Me_xO_y had good stability and activity at relatively low temperatures, which provided the basis for further pilot-scale study for potential industrial applications.

Conflict of Interest

The authors declare no conflict of interest.

References

- SÁDOVSKÁ G., TABOR E., SAZAMA P., LHOTKA M., BERNAUER M., SOBALÍK Z. High temperature performance and stability of Fe-FER catalyst for N₂O decomposition. *Catal. Commun.* **89**, 133, **2017**.
- ABU-ZIED B. M., SOLIMAN S. A., ABDELLAH S. E. Enhanced direct N₂O decomposition over Cu_xCo_{1-x}Co₂O₄ (0.0 ≤ x ≤ 1.0) spinel-oxide catalysts. *J. Ind. Eng. Chem.* **21**, 814, **2015**.
- PARK S., CHOI J.H., PARK J. The estimation of N₂O emissions from municipal solid waste incineration facilities: The Korea case. *Waste Manage.* **31**, 1765, **2011**.
- MASSARA T.M., MALAMIS S., GUIASOLA A., AEZA J.A.B., NOUTSOPOULOS C., KATSOU E. A

- review on nitrous oxide (N_2O) emissions during biological nutrient removal from municipal wastewater and sludge reject water. *Sci. Total Environ.* **596-597**, 106, **2017**.
5. CHIPPERFIELD M.P., BEKKI S., DHOMSE S., HARRIS N.R.P., HASSLER B., HOSSAINI R., STEINBRECHT W., THIÉBLEMONT R., WEBER M. Detecting recovery of the stratospheric ozone layer. *Nature* **549**, 211, **2017**.
 6. DHAL G.C., MOHAN D., PRASAD R. Preparation and application of effective different catalysts for simultaneous control of diesel soot and NO_x emissions: An overview. *Catal. Sci. Technol.* **7**, 1803, **2017**.
 7. REVELL L.E., TUMMON F., SALAWITCH R.J., STENKE A., PETER T. The changing ozone depletion potential of N_2O in a future climate. *Geophys. Res. Lett.* **42**, 10047, **2015**.
 8. RAVISHANKARA A.R., DANIEL J.S., PORTMANN R.W. Nitrous oxide (N_2O): The dominant ozone-depleting substance emitted in the 21st century. *Science* **326**, 123, **2009**.
 9. YU H.B., WANG X.P. Apparent activation energies and reaction rates of N_2O decomposition via different routes over Co_3O_4 . *Catal. Commun.* **106**, 40, **2018**.
 10. GALLE M., AGAR D.W., WATZENBERGER O. Thermal N_2O decomposition in regenerative heat exchanger reactors. *Chem. Eng. Sci.* **56**, 1587, **2001**.
 11. PEREZ-RAMIREZ J., KAPTEIJN F., SCHOFFEL K., MOULIJN J.A. Formation and control of N_2O in nitric acid production: Where do we stand today?. *Appl. Catal. B: Environ.* **44**, 117, **2003**.
 12. PINAEVA L.G., PROSVIRIN I.P., DOVLITOVA L.S., DANILOVA I.G., SADOVSKAYA E.M., ISUPOVA L.A. MeO_x/Al_2O_3 and MeO_x/CeO_2 ($Me=Fe, Co, Ni$) catalysts for high temperature N_2O decomposition and NH_3 oxidation. *Catal. Sci. Technol.* **6**, 2150, **2016**.
 13. PEREZ-ALONSO F.J., MELIAN-CABRERA I., GRANADOS M.L., KAPTEIJN F., FIERRO J.L.G. Synergy of $Fe_xCe_{1-x}O_2$ mixed oxides for N_2O decomposition. *J. Catal.* **239**, 340, **2006**.
 14. HABER J., NATTICH M., MACHEJ T. Alkali-metal promoted rhodium-on-alumina catalysts for nitrous oxide decomposition. *Appl. Catal. B: Environ.* **77**, 278, **2008**.
 15. LI L.L., MENG Q.L., WEN J.J., WANG J.G., TU G.M., XU C.H., ZHANG F.M., ZHONG Y.J., ZHU W.D., XIAO Q.X. Improved performance of hierarchical Fe-ZSM-5 in the direct oxidation of benzene to phenol by N_2O . *Microporous Mesoporous Mater.* **227**, 252, **2016**.
 16. CHATZIIONA V.K., CONSTANTINOU B.K., SAVVA P.G., OLYMPIOU G.G., KAPNISIS K., ANAYIOTOS A., COSTA C.N. Regulating the catalytic properties of Pt/ Al_2O_3 through nanoscale inkjet printing. *Catal. Commun.* **103**, 69, **2018**.
 17. PIETROGIACOMI D., CAMPA M.C., CARBONE L.R., TUTI S., OCCHIUZZI M. N_2O decomposition on CoO_x , CuO_x , FeO_x or MnO_x supported on ZrO_2 : The effect of zirconia doping with sulfates or K^+ on catalytic activity. *Appl. Catal. B: Environ.* **187**, 218, **2016**.
 18. JABŁOŃSKA M., PALKOVITS R. It is no laughing matter: nitrous oxide formation in diesel engines and advances in its abatement over rhodium-based catalysts. *Catal. Sci. Technol.* **6**, 7671, **2016**.
 19. AMROUSSE R., TSUTSUMI A., BACHAR A. Retracted article: A novel approach for N_2O decomposition over Rh-substituted hexaaluminate catalysts. *Catal. Sci. Technol.* **3**, 576, **2013**.
 20. DACQUIN J.P., DUJARDIN C., GRANGER P. Catalytic decomposition of N_2O on supported Pd catalysts: Support and thermal ageing effects on the catalytic performances. *Catal. Today* **137**, 390, **2008**.
 21. BEYER H., EMMERICH J., CHATZIAPOSTOLOU K., KÖHLER K. Decomposition of nitrous oxide by rhodium catalysts: Effect of rhodium particle size and metal oxide support. *Appl. Catal. A: Gen.* **391**, 411, **2011**.
 22. YENTEKAKIS I.V., GOULA G., PANAGIOTOPOULOU P., KAMPOURI S., TAYLOR M., KYRUAKOU G., LAMBERT R. Stabilization of catalyst particles against sintering on oxide supports with high oxygen ion lability exemplified by Ir-catalyzed decomposition of N_2O . *Appl. Catal. B: Environ.* **192**, 357, **2016**.
 23. LIN J., PAN X.L., WANG X.D., CONG Y., ZHANG T., ZHU S.M. Catalytic decomposition of propellant N_2O over Ir/ Al_2O_3 catalyst. *AIChE J.* **62**, 3973, **2016**.
 24. ABU-ZIED B.M., BAWAKED S.M., KOSA S.A., ALI T.T., SCHWIEGER W., AQLAN F.M. Effects of Nd-, Pr-, Tb- and Y-doping on the structural, textural, electrical and N_2O decomposition activity of mesoporous NiO nanoparticles. *Appl. Surf. Sci.* **419**, 399, **2017**.
 25. BASAHEL S.N., ABD EL-MAKSOD I.H., ABU-ZIED B.M., MOKHTAR M. Effect of Zr^{4+} doping on the stabilization of ZnCo-mixed spinel system and its catalytic activity towards N_2O decomposition. *J. Alloys Compd.* **493**, 630, **2010**.
 26. YAN L., REN T., WANG X.L., GAO Q., JI D., SUO J.S. Excellent catalytic performance of $Zn_xCo_{1-x}Co_2O_4$ spinel catalysts for the decomposition of nitrous oxide. *Catal. Commun.* **4**, 505, **2003**.
 27. EOM W.H., AYOUB M., YOO K.S. Catalytic decomposition of N_2O at low temperature by reduced cobalt oxides. *J. Nanosci. Nanotechnol.* **16**, 4647, **2016**.
 28. KIM M.J., LEE S.J., RYU I.S., JEON M.W., MOON S.H., ROH H.S., JEON S.G. Catalytic decomposition of N_2O over cobalt based spinel oxides: The role of additives. *Mol. Catal.* **442**, 202, **2017**.
 29. ZHANG J.L., HU H., XU J., WU G.M., ZENG Z.W. N_2O decomposition over K/Na-promoted Mg/Zn-Ce-cobalt mixed catalysts. *J. Environ. Sci.* **26**, 1437, **2014**.
 30. GRZYBEK G., STELMACHOWSKI P., INDYKA P., INGER M., WILK M., KOTARBA A., SOJKA Z. Cobalt-zinc spinel dispersed over cordierite monoliths for catalytic N_2O abatement from nitric acid plants. *Catal. Today* **257**, 93, **2015**.
 31. ZABILSKIY M., DJINOVIC P., ERJAVEC B., DRAZIC G., PINTAR A. Small CuO clusters on CeO_2 nanospheres as active species for catalytic N_2O decomposition. *Appl. Catal. B: Environ.* **163**, 113, **2015**.
 32. LIU Z.M., HE C.X., CHEN B.H., LIU H.Y. CuO- CeO_2 mixed oxide catalyst for the catalytic decomposition of N_2O in the presence of oxygen. *Catal. Today* **297**, 78, **2017**.
 33. KONSOLAKIS M., CARABINEIRO S.A.C., PAPISTA E., MARNELLOS G.E., TAVARES P.B., AGOSTINHO MOREIRA J., ROMAGUERA-BARCELAY Y., FIGUEIREDO J.L. Effect of preparation method on the solid state properties and the deN_2O performance of CuO- CeO_2 oxides. *Catal. Sci. Technol.* **5**, 3714, **2015**.
 34. ZHENG X.Y., ZHANG R.H., BAI F., HUA C., WANG S.B., DUAN X.G. Catalytic decomposition of N_2O over Cu-Zn/ $ZnAl_2O_4$ catalysts. *Catalysts* **7**, 1, **2017**.
 35. LIU Z.M., ZHOU Z.Z., HE F., CHEN B.H., ZHAO Y.Y., XU Q. Catalytic decomposition of N_2O over NiO- CeO_2 mixed oxide catalyst. *Catal. Today* **293-294**, 56, **2017**.